ORNL/TM-2016/460

Light Water Reactor Sustainability Program

Development of Computational Tools for Predicting Thermal- and Radiation-Induced Solute Segregation at Grain Boundaries in Fe-based Alloys

September 2016

U.S. Department of Energy

Office of Nuclear Energy

ORNL/TM-2016/460

Development of Computational Tools for Predicting Thermal- and Radiation-Induced Solute Segregation at Grain Boundaries in Fe-based Alloys

Ying Yang

09/2016

Prepared for the
U.S. Department of Energy
Office of Nuclear Energy

ABSTRACT

Radiation induced segregation (RIS) has been frequently reported in structural materials such as austenitic, ferritic, and ferritic-martensitic stainless steels (SS) that have been widely used in light water reactors (LWRs). RIS has been linked to secondary degradation effects in SS including irradiation induced stress corrosion cracking (IASCC). Earlier studies on thermal segregation in Fe based alloys found that metalloids elements such as P, S, Si, Ge, Sn etc. embrittle the materials when enrichment was observed at grain boundaries (GBs). RIS of Fe-Cr-Ni based austenitic steels has been modeled in the U.S. 2015 fiscal year (FY2015), which identified the pre-enrichment due to thermal segregation can have an important role on the subsequent RIS. The goal of this work is to develop thermal segregation models for alloying elements in steels for future integration with RIS modeling.

Thermal segregation and RIS of P in α iron and various steels has been extensively studied and therefore has been chosen as the first element to study. The current approach integrated computational thermodynamics with GB segregation modeling to study thermal equilibrium segregation of solute atoms in α iron in Fe-P, Fe-C-P and Fe-M-P and Fe-M-C-P (M=Cr, Mn, Ni, Mo, Nb, Ti) alloys. The following factors were considered during the modeling: effect of M on the solubility of P in α_Fe; the chemical interaction between Fe-M and M-P; the competition between C and P of GB sites; effect of M on the solubility of C in α_Fe; combined effect of C and M on the P segregation. The major outcomes from this work are:

1) Multicomponent thermodynamic database of Fe-M-C-P (M=Cr, Mn, Ni, Mo, Nb, Ti) has been compiled and developed based on critically assessed literature data. This database provided major thermodynamic inputs for thermal GB segregation model.
2) The McLean equation was used to describe the GB segregation of an ideal solid solution, and the Guttmann's equation was used to describe the GB segregation of non-ideal solid solution of multicomponent alloys.
3) For different alloying additions (M=Cr, Mn, Ni, Mo, Nb, Ti), the solubility of P in α_Fe was systematically evaluated, and the solid solution behavior of Fe-M and M-P was also assessed to provide guidance on the selection of GB segregation model.
4) Among the six alloying elements (M=Cr, Mn, Ni, Mo, Nb, Ti), Mn and Ni do not affect the P segregation. The currently used intrinsic segregation energy of Mn and Ni suggests that they do not segregate at GBs. Cr and Mo do not affect the segregation of P either, however, unlike Mn and Ni, they will enrich at GBs due to positive or repulsive interaction with the matrix Fe atoms. Nb and Ti greatly reduces the P segregation due to the very strong scavenging effect. The remaining Nb and Ti in α_Fe are so small that they were not included in GB segregation modeling.
5) C strongly affects the P segregation, by competing with P for GB sites. Additions of alloying elements such Cr, Ni, Mn, Mo, Nb and Ti, on one hand, can scavenge the C atoms in solid solution by forming M carbides. Less C in solid solution leads to weaker competition of C for GB sites, thereby promoting the segregation of P. On the other hand, these metal additions may simultaneously reduce the P solubility by forming metal

phosphides, which helps to suppress the P segregation. Therefore, P segregation displays a more complex behavior in the Fe-M-C-P systems.

ACKNOWLEDGEMENTS

This work was supported by the U.S. Department of Energy (DOE), Office of Nuclear Energy, Light Water Reactor Sustainability (LWRS) Research and Development Effort, under contract DE-AC05-00OR22725 with UT-Battelle, LLC. Discussions with Drs. J.T. Busby, K. Field and K. Leonard at ORNL and Dr. Pavel Lejček at Institute of Physics of Academy of Sciences of the Czech Republic are acknowledged.

CONTENTS

FIGURES

ACRONYMS

SS: Stainless Steels

RIS: Radiation Induced Segregation

GB: Grain Boundary

GBST: Grain Boundary Segregation Transition

IASCC: Irradiation Induced Stress Corrosion Cracking

LWRs: Light Water Reactors sustainability

CT: Computational Thermodynamics

CALPHAD: CALculation of PHAse Diagram

1. Introduction

Structural materials such as austenitic, ferritic, and ferritic-martensitic stainless steels (SS) are widely used in light water reactors (LWRs). However, the combined long-term neutron irradiation and thermal conditions impose great challenges on the stability of materials. For example, a variety of microstructural and microchemical changes have been reported in austenitic SS core internals of LWRs, primarily including a high density (10^{22}–10^{23} m^3) of Frank loops (< approximately 20 nm), precipitates (e.g., Ni/Si-rich γ', G-phases and carbides), and cavities, as well as chemical segregation at grain boundaries (GBs) and dislocations [1-5]. These changes lead to material degradation such as irradiation-assisted stress corrosion cracking (IASCC). IASCC has been linked to the depletion of Cr at the grain boundary as a result of radiation-induced segregation (RIS) [2]. RIS modeling of Fe-Cr-Ni system has been subjected to several prior studies [6-13]. Recently, Yang et al. [14] has developed an improved RIS model based on Perks model [15] by integrating computational thermodynamics (CT) [16] into the modeling of compositional dependent diffusion coefficients and thermodynamic factors, and interstitial binding model [13] into the modeling diffusion flux of interstitials. One of the major findings resulted from the improved model is that the elemental segregation in the steady state is the result of not only preferential coupling of elements with defects but also the composition gradient in the vicinity of the grain boundary that was formed during the transient state. The latter is the major cause for the oscillatory behavior of segregation profile (such as a W-shape) in the vicinity of the GB. While the previous study shows the composition gradient that formed from the transient state has an important role in the steady-state microchemistry at defect sinks, Busby et al. [17] found that the pre-existing Cr-enrichment at grain boundary due to thermal segregation also leads to the oscillatory behavior of segregation profiles during the subsequent irradiation. Similarly, Cole et al. [18] found Cr, Mo and P in 316SS under different cooling rates had already enriched to various levels at grain boundary before the materials being exposed to irradiation environments. The higher the enriched levels lead to the more pronounced W-shape profile during the subsequent irradiation. Nastar et al. [19] did a mean-field RIS kinetics simulation and also found a W-shape profile of Cr when using a pre-enriched Cr profile as input. It becomes evident that pre-enrichment of element at GBs due to thermal segregation has an important role in determining the subsequent RIS profile as well as the microchemistry at GBs [17-19].

Earlier studies on thermal segregation of metalloid impurities in Fe based alloys found that metalloids elements such as P, S, Si, Ge, Sn etc. embrittle the materials when they enrich at grain boundaries [20]. For FY 2016, this work aims at developing a computational model to describe thermodynamics and kinetics of thermal segregation of alloying elements in steels. In FY 2017, this thermal segregation modeling will be coupled with the RIS modeling to provide a complete description of complicated, multi-elemental segregation under both irradiation and thermal conditions.

2. Literature review on experimental data

Among various elements, thermal segregation of phosphorus at GBs of ferritic alloys is one of the most widely studied subjects and has been known as a primary contributor to the temper embrittlement of low-alloying steels [21-28]. Not only thermal segregation, the irradiation enhanced P segregation at GBs has been also connected with irradiation enhanced embrittlement of pressure vessel steels of nuclear reactors [29-35]. Therefore, thermal segregation of P in

ferritic alloys was selected to be investigated using the currently developed models. Detailed literature review on P segregation in the Fe-P binary, Fe-C-P, Fe-M-P ternary and Fe-M-C-P quaternary (M=Cr, Ni, Mn, Mo, Nb and Ti) is given below.

2.1 The Fe-P binary

Quantitative measurements on GB segregation levels of P in α-Fe have been mainly using AES (Auger Electron Spectroscopy) in literature, however, the results differ greatly from one work to another. Ramasubramanian and Stain [36] suggested the P concentration at GBs can be as high as 100 at%. Matsuyama and Suto [37] performed the systematic quantitative AES (Auger Electron Spectroscopy) analysis on GB segregation of P for Fe-(0.05~1.7) wt% P alloys quenched from the temperature ranging from 1150 to 500ºC for different time periods. They found that in low P alloys the segregation levels of P at GBs increased proportionally with the bulk concentration and inversely with the temperature from which the alloys were quenched. The enrichment ratio was on the order of ten. In high P alloys the P segregation is saturated at about 15 at%. Erhart and Grabke [22], based on AES results, derived GB composition of P in a series of Fe-P alloys, with P concentration from 0.003 to 0.33 wt%. While they also found that the segregation levels of P at GBs increased proportionally with the bulk concentration and inversely with the quenching temperature, the enrichment ratio was on the order of hundred, much higher than that was found in Matsuyama and Suto's work. Such drastic difference in the GB composition measurement is likely due to the different methods that were used to convert the peak height ratio in AES spectrum into the composition. Erhart and Grabke [22] used the peaks of P(120eV) and Fe(650eV) and a simple linear relationship between the peak height and GB concentration $I_P/I_{Fe}=C_P/C_{Fe}$. Matsuyama and Suto [37] used the peaks of P(120eV) and Fe(703eV), and derived the GB composition from the peak ratio through a sophisticated formula based on the calibration curve and depth effect. Additionally, instead of reporting the GB composition, Oku and Suzuki [38]reported the AES peak height ratio between P (120eV) and Fe (703eV) at transgranular and intergranular fracture surfaces.

Suzuki and colleagues [26, 38, 39] published a series of papers on the chemical state of P segregated at GBs of α_Fe, using combination of AES with XPS (X-ray Photoelectron Spectroscopy) or EELS (Electron Energy-Loss Spectroscopy). They found that P segregated at GBs of α_Fe is in the same chemical state as P in Fe_3P. However, instead of forming 3D Fe_3P precipitates, the segregated P at GBs should be considered as a 2D phase because it has a thickness of a few atomic layers from the surface. The same results were obtained for segregated P in an Fe-0.1wt%P and an Fe-0.05wt%P alloys that had undergone the same experimental procedure. Their results can be confirmed by Egert and Panzner's work [40]. Hashimoto [41, 42] and Ishida [43] preformed atomistic simulation on structural transition at GBs due to P segregation, and confirmed that the local atomic environment surrounding P atoms is similar to that of the crystalline Fe_3P. Both XPS and atomistic simulation results supported that the bonds of P atoms with surrounding Fe atoms at GBs are of covalent nature.

In view of the large difference in the reported GB compositions, we compared the raw AES peak height ratio in Figure *1*. The open symbols represent data from transgranular fracture surface, which shows good agreements between different authors. The solid symbols represent data from intergranular surface. These data differ greatly from one work to another. Such difference may be contributed from different grain boundary structures. However, in general it was found that the P segregation at GB at low temperature is larger than those at high temperature. Among different works, Erhart [22] and Matsuyama [37] generated large datasets

for different compositions at different temperatures. To minimize the uncertainties due to different conversion methods, a standard approach in the AES analysis handbook [44] was used to convert the AES peak ratio to the composition, i.e.,

$$\frac{C_P}{C_{Fe}} = \frac{I_P}{I_{Fe}} \times \frac{S_{Fe}}{S_P} \quad (1)$$

S_i is the sensitivity factor of element i. Both Erhart [22] and Matsuyama [37]'s work used 3KeV beam, at which the sensitivity factor of P at 120eV is 3.0834, and that is 0.7878 for Fe 650eV and 0.9494 for Fe 703eV. Inserting these factors into Eq. (1), the raw peak ratio can be converted into the composition, as shown in the right Y scale in Figure *1*. It shows that maximum composition is no more than 0.25 (mol. fraction) which is drastically different from that originally reported by Erhart and Grabke [22]. More importantly, this result is consistent with the chemical state of saturated P at GBs in the form of Fe_3P.

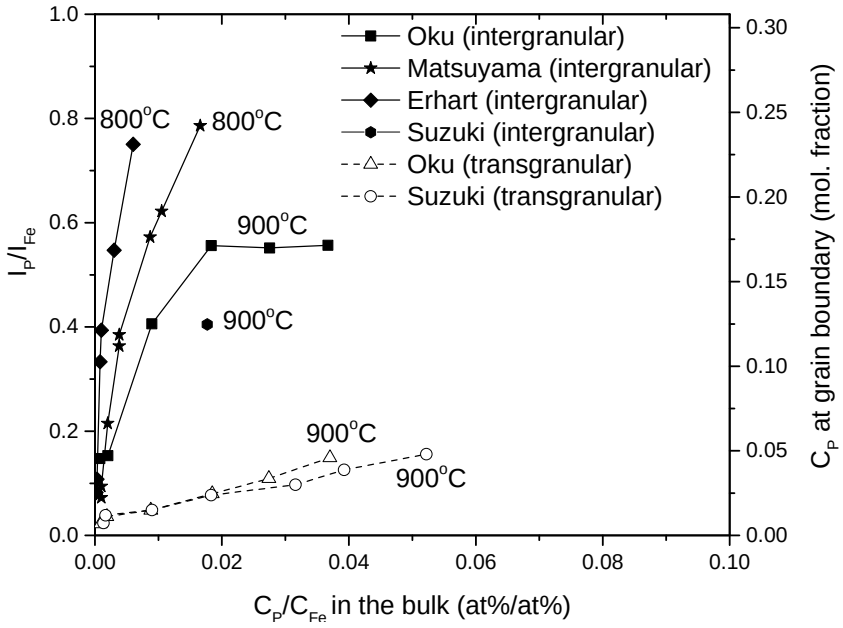

Figure 1 Literature data on raw AES peak height ratio of P and Fe in Fe-P alloys and derived P composition at GBs using the standard approach in the AES analysis handbook [44]. Note: Temperature in this figure refers to annealing temperature from which the samples were quenched.

Based on the analysis above, we assume that the GB compositions of P reported by Erhart and Grabke [22] are not true compositions of P. They represent the coverage of Fe_3P at GBs. The true P composition can be calculated from the Fe_3P coverage through the following equation.

$$x_P = \frac{x_{Fe_3P}}{1+3x_{Fe_3P}} \quad (2)$$

When x_{Fe_3P} equals to 1, the x_P equals to 0.25. Then, we compared the P composition derived from Eq. (1) with those from Eq. (2) in Figure *2*. Now, the data from these two methods are in excellent agreement.

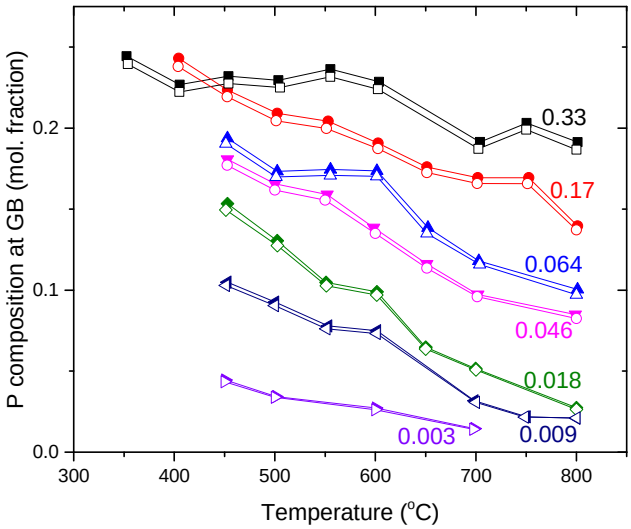

Figure 2 Comparison of GB compositions of P derived from Eqs. (1) (open symbols) and (2) (solid symbols).

2.2 The Fe-C-P, Fe-M-P ternary and Fe-M-C-P quaternary (M=Cr, Ni, Mn, Mo, Nb and Ti)

Additional alloying elements make the phosphorus segregation more complicated. They can have multiple effects [45]. First, they can change the solubility of P in the matrix due to the scavenging and gettering effect and form precipitates. Second, for an ideal solid solution, the additional elements can reduce the segregation of P by segregating and competing with P for available GB sites. Third, for a non-ideal solid solution, the chemical interaction between additional elements and P can alter the diffusion and segregation energy.

C, Cr, Ni, Mn, Mo, Nb and Ti are common alloying elements in the Fe-based alloys, therefore, the segregation of these elements and their effects on the segregation of P were included in the current modeling. Experimental segregation data in the Fe-C-P and Fe-M-P ternary and Fe-M-C-P quaternary systems are briefly reviewed here and more details will be described in Section of results and discussion. Carbon is a good example to demonstrate the site competition mechanism. Erhart and Grabke [22] studied the competition between C and P. They found that P segregation decreases with increasing C, until the solubility of C in Fe is reached. Further increase of C beyond the solubility won't change the segregation, i.e., reaching the plateau. The site competition mechanism assumes no interaction between C and P. They compete for a limited number of sites and their segregation tendency is given by constant values of their segregation free energies. Nb and Ti can be well classified into the category for scavenging and gettering effect due to the formation of precipitates or clusters of metal phosphides [46]. Their roles are mainly to scavenge and getter P, thereby lowering the concentration of P in Fe. Therefore, addition of Nb and Ti in general reduces the segregation P. Ti is more effective than Nb in suppressing the P segregation because of higher affinity for P. The third category of alloying elements are those having chemical interactions with P. They may affect the segregation thermodynamics and/or kinetics of P. In studying the Fe-Cr-P system, Erhart and Grabke [22] found that Cr did not affect the segregation of P, but the Cr itself enriched at GBs. Mo is also found to be slightly enriched at GBs without

enhancing the segregation of P [46]. Guttmann et al.[23] studied thermodynamics of interactive co-segregation of P and Cr, Mn, Ni and Mo in temper-brittle steels. They found the all these elements enriched at GB. Based on co-segregation model, they suggested that Cr, Ni, Mn and Mo possess a small intrinsic segregation energy and the strong chemical interaction between metal alloying elements and phosphorus. However, their conclusion didn't find support from other work [47, 48]. Doig and Flewitt [47] studied the GB segregation of Fe-Ni-P alloys using Scanning Transmission Electron Microscopy (STEM), and found while the P segregated at GB, there was no measurable change in Ni concentration from bulk to grain boundary. For the Mn effect, while there is an agreement than Mn segregation to the GB is observed, there is no consistent evidence for an enhancement of P-segregation by the segregated Mn [48-50]. Tatsumi et al. [51] reported no effect of Mn on the GB segregation of P in the range of 0.5 to 1.5wt% Mn. Grabke et al. [50] reported no effect of Mn on the GB segregation of P in the range of 0.5 to 9.4wt% Mn. Since the materials in Guttmann's work [23] are real steels in which many impurity elements are present, they have more complex interaction between alloying elements and impurities. In this work, most experimental results were taken from Grabke et al's work [22, 45, 46, 50] for comparison and validation because they used model alloys with well controlled chemistry.

In real steels, C is a common element in steels. Therefore, it is necessary to consider P and C segregation simultaneously. Addition of alloying elements such Cr, Ni, Mn, Mo, Nb and Ti has profound effect on carbon activity, and subsequently on the C and P segregation. It has been found that the Cr addition increases the P segregation [22], which was interpreted as that Cr has strong affinity with C, thereby reducing the C in the matrix and weakening the capability of C competition with P at the GB sites. Mn has been found to work similarly as Cr in binding C atoms and promoting P segregation[50]. In experimental study of the Fe-Nb-C-P and Fe-Ti-C-P alloys [46, 52], a maximum P segregation was found at a critical level of C content for a fixed Nb(Ti) and P content. When the C content is smaller than the critical level, P segregation drastically increases with increasing C content. When the C content is larger than the critical level, P segregation decreases with increasing C content until reaches a plateau. The critical level corresponds to the solubility of C in α_Fe.

While the reported experimental results on P segregation at the GB of ferritic alloys differ from one work to the other, due to the presence of other impurity elements, the different cooling rates (eg., furnace cooling or water quench) and aging periods, the method of analyzing the AES data, etc., there are general trends that can be captured from the experimental results, as summarized in the following: 1) The segregation levels of P increases proportionally with the bulk concentration; 2) The segregation levels of P decreases with the increasing aging temperature; 3) The chemical state of P at GB is dominated by Fe_3P; 4) P segregation at GBs occurs in merely a few or even only one atomic layer; 5) Both small angle and low Σ symmetric boundaries correspond to low levels of P segregation. Although the grain boundary structure has an important role in the segregation process, the current modeling will focus on thermodynamic and kinetic aspects of P segregation at random high angle GBs, where the segregation level is the greatest. The future refinement of the current models will include the GB structure modeling such as the work of Field et al. [7].

3. Modelling methodology and theory

The modelling methodology is schematically shown in Figure *3*. Thermal induced segregation starts with the modeling of thermodynamic properties of relevant alloy systems and the GB segregation energy of elements in the relevant solid solution, which will then be input to the McLean and/or Guttmann models to calculate equilibrium segregation. The equilibrium segregation defines the boundary conditions of subsequent kinetics simulation. On the other hand, radiation induced segregation starts with rate theory that describes the defect production, recombination and annihilation, and preferential coupling between solute atoms and defects. The combined effect of thermal and radiation will affect the diffusivity, the boundary conditions, and the atomic fluxes. In FY 2015, an improved RIS model based on Perks model [15] has been developed for the Fe-Cr-Ni alloys through the LWRs support, by integrating computational thermodynamics (CT) [16] into the modeling of compositional dependent diffusion coefficients and thermodynamic factors, and interstitial binding model [13] into the modeling diffusion flux of interstitials. The focus of this year (FY2016) is to develop a thermal induced segregation model. The RIS model and TIS model will be integrated in FY2017. The modeling theories and tools for thermal segregation are described in details in Sections 3.1 and 3.2.

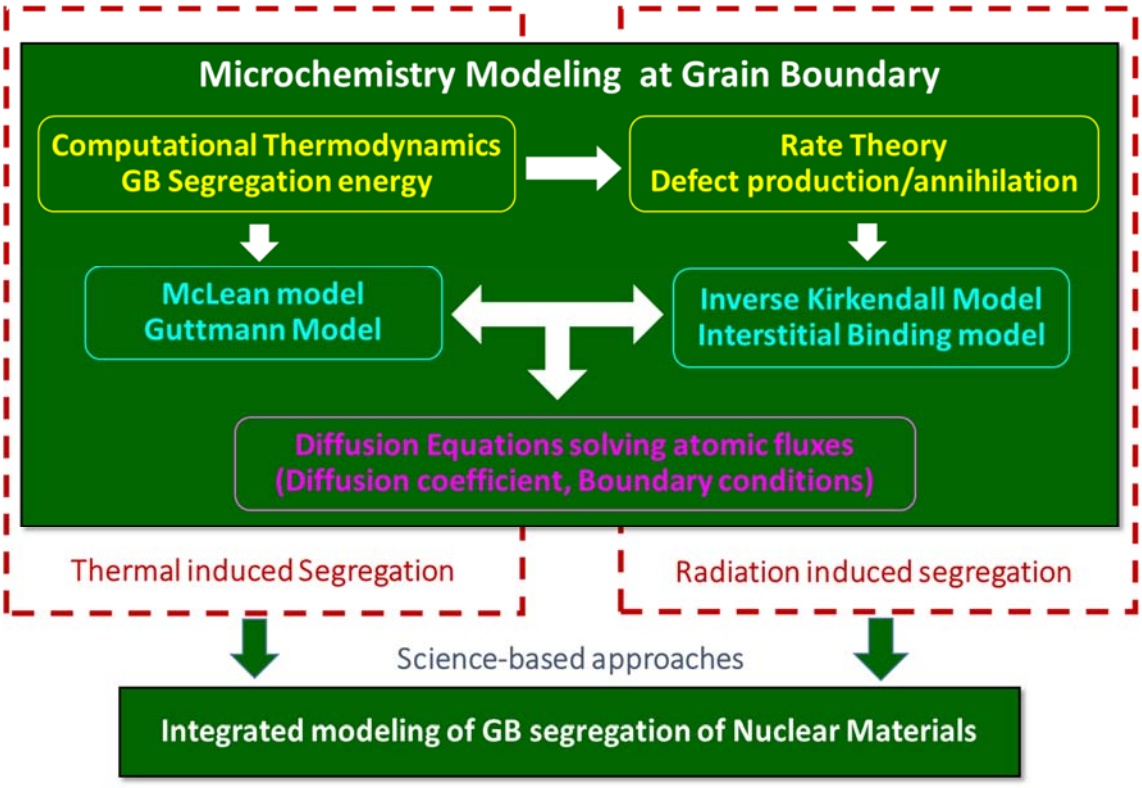

Figure 3 Schematic frame work of integrated modeling of GB segregation in nuclear materials

3.1 Thermodynamic model

3.1.1 McLean equation

McLean [53] developed a theory to describe the thermodynamics of equilibrium segregation. The McLean segregation equation describes the relationship between surface composition, bulk

composition and segregation energy. For an Fe-P system, with Fe as the solvent and P as the solute, the surface composition is described as Eq. (3):

$$\frac{x_P^{\varphi}}{1-x_P^{\varphi}} = \frac{x_P}{1-x_P} exp(\frac{\Delta G_P}{RT}) \qquad (3)$$

x_P^{φ} is the surface composition and x_P is the bulk composition. ΔG_P is the segregation energy. R is gas constant and T is temperature in Kelvin. The McLean equation has two assumptions: 1) the segregated atoms are non-interacting, and 2) the components have equal atomic size. The McLean equation is generally applied to a dilute solution where the x_P is neglible. For a ternary dilute system with negligible chemical interaction between solute elements, the segregation of solute follows the site competition mechanism described by an extended McLean equation. Using Fe-C-P as an example, the surface composition can be described as Eq. (4a):

$$\frac{x_P^{\varphi}}{1-x_P^{\varphi}-x_C^{\varphi}} = \frac{x_P}{1-x_P-x_C} \exp(\frac{\Delta G_P^0}{RT}) \quad (4a)$$

$$\frac{x_P^{\varphi}}{1-x_P^{\varphi}-x_C^{\varphi}} = \frac{x_C}{1-x_P-x_C} \exp(\frac{\Delta G_C^0}{RT}) \quad (4b)$$

When chemical interactions occur in between solute atoms, additional terms are needed. Take a binary as an example, Fowler [54] introduced interaction energy (Ω) between adjacent adsorbate atoms into segregation energy such that they attract (negative Ω) or repel (positive Ω) each other. The general formula of Fowler segregation model is described by Eq. (5):

$$\frac{x_P^{\varphi}}{1-x_P^{\varphi}} = \frac{x_P}{1-x_P} \exp(\frac{\Delta G_P + \Omega x_P^{\varphi}}{RT}) \qquad (5)$$

If Ω is zero, the Fowler equation reduces to the McLean equation. As Ω becomes more and more positive the segregation shows progressively sharper rises as the temperature falls until eventually the rise in segregation is discontinuous at a certain temperature. An analog is an immiscibility gap in a phase diagram. Such a discontinuity can be correlated with the concept called grain boundary segregation transition (GBST) at which the solute coverage at GBs changes from a low segregated state to a high segregated state.

3.1.2 Guttmann's equation

Guttmann [55] developed a GB segregation model for a multicomponent system, assuming the interaction between elements follows the regular solid solution. The GB composition of a solute i in a multicomponent system can be written as Eq. (6):

$$x_i^{\varphi} = \frac{x_i \exp(\frac{\Delta G_i^{Seg}}{RT})}{1-\sum_{i\neq Fe} x_i + \sum_{i\neq Fe} x_i \exp(\frac{\Delta G_i^{Seg}}{RT})} \qquad (6)$$

"i" and "Fe" respectively denote alloying and matrix elements. When there is only one alloying element i, the Guttmann's model can be reduced to the McLean's model. Although the Guttmann's segregation equation resembles the McLean's, there is a major difference between the McLean's and Guttmann's model. ΔG_P in the McLean equation is independent of composition x_P^{φ}, because of the assumption of no interaction between elements. However, in

Guttmann's equation, the segregation energy of an individual element is a function of composition. The compositional dependency of solute in a binary is described as Eq. (7):

$$\Delta G_i = \Delta G_i^0 + 2L_{Fei}(x_i^{\varphi} - x_i^B) \qquad (7)$$

ΔG_i^0 is the segregation energy in the respective *Fe-i* binary, which is independent of composition. L_{Fei} is the regular interaction parameter between Fe and i. The second term in Eq. (7) can be closely related to Fowler's term in Eq. (5). When L_{FeI} is positive, meaning repulsive force between Fe and i, and when it is negative, meaning attractive force between them. This equation also suggested that for a non-ideal solution, i.e., $L_{Fei} \neq 0$, the segregation energy is composition dependent. For a dilute solution x_i^B, $x_i^B \approx 0$. Therefore, only when x_i^{φ} is also close to zero, the interaction term can be ignored. However, in literature, the segregation energy of most dilute systems that were fitted into the McLean's method are composition independent, even though x_i^{φ} was often found to be quite large. Therefore, the experimentally derived segregation energy in these dilute systems is an average quantity in terms of composition, which takes both terms in Eq. (4) into consideration. In a ternary Fe-M-P, the segregation energy of P and M is described by Eqs. (8a~8b), respectively:

$$\Delta G_P = \Delta G_P^0 + 2L_{FeP}\left(x_P^{\varphi} - x_P^B\right) + (L_{FeP} + L_{FeM} - L_{MP})(x_M^{\varphi} - x_M^B) \qquad (8a)$$

$$\Delta G_M = \Delta G_M^0 + 2L_{FeM}\left(x_M^{\varphi} - x_M^B\right) + (L_{FeP} + L_{FeM} - L_{MP})(x_P^{\varphi} - x_P^B) \qquad (8b)$$

Based on Eqs. (8a~8b), the segregation of M and P depends on the complex relationship among ΔG_P^0, ΔG_M^0, L_{FeM}, L_{FeP}, $(L_{FeM} + L_{FeP} - L_{MP})$. In this work, the ΔG_M^0 and ΔG_P^0 in this work were adopted from literature data [22, 56] and the interaction parameters were taken from thermodynamic modeling.

3.1.3 Butler's equation

Kaptay [57] recently modeled the phosphorus GB segregation using the Butler model [58]. The Butler's model is essentially the Guttmann's model, but originally developed for the surface tension of liquid solution. In the McLean's equation, the GB energy is implicitly included in Eq. (3). While in Bulter's equation, the surface energy was explicitly described as Eq. (9)

$$\sigma_i = \sigma_i^0 + \frac{RT}{\omega_i}\ln\left(\frac{x_i^{\varphi}}{x_i}\right) + \frac{\Delta G_i^{E,\varphi} - \Delta G_i^E}{w_i} \qquad (9)$$

$$\Delta G_i^{\varphi} = RTln\left(x_i^{\varphi}\right) + \Delta G_i^{E,\varphi} \qquad (10)$$

$$\Delta G_i = RTln(x_i) + \Delta G_i^E \qquad (11)$$

σ_i^0 is the surface energy of pure element i. ω_i is the molar interfacial energy. $\Delta G_i^{E,\varphi}$ and ΔG_i^E are the partial molar excess mixing Gibbs energy of component "*i*" in the GB and bulk region, respectively. Assuming regular solution, the excess energy can be described as Eqs. (10~11):

$$\Delta G_i^{E,\varphi} = \beta\Omega(1 - x_i^{\varphi})^2 \qquad (12)$$

$$\Delta G_i^E = \Omega(1 - x_i)^2 \qquad (13)$$

The interaction energy (Ω) is the same term as that in the Fowler's term. β is the ratio of unbroken bonds in the GB region compared to the bulk grain.

In Kaptay's work, instead of choosing P, Fe_3P was chosen as the segregation species, He gave the reason as the segregation usually occurs in a system with phase separation, i.e., a system with a positive mixing energy to form a solution. However, in Fe-P system, the mixing energy in body centered cubic (BCC) solid solution of Fe and P is negative, suggesting no segregation should occur. Nevertheless, if the negative mixing energy was used to create the Fe_3P cluster, and if the interaction energy between Fe and Fe_3P is positive, then the segregation of P should occur in the form of Fe_3P. His model was able to reasonably describe the P segregation at 1450°C, and predict a grain boundary segregation transition at which point the coverage of Fe_3P goes from a low segregated state to a high segregated state.

Detailed thermodynamic and kinetic modeling on P segregation at GB in α_Fe has been developed and compared for using the McLean equation and the Kaptay's approach in previous work [59]. The McLean approach can reasonably describe most experimental data except for the extremely low P alloys at very low temperature due to sluggish kinetics. On the other hand, the Kaptay's approach requires known thermodynamic and thermophysical knowledge for pure components to calculate the surface energy. Unfortunately, most of these data are not available, which limits its application in multi-component systems. In this work, we will describe thermal segregation by extending the Mclean's equation to a multicomponent system with negligible chemical interaction and using Guttmann's equation to those with appreciable chemical interaction.

3.2 Kinetics model

Materials thermodynamics dictated the maximum solute segregation at GBs, however, it cannot tell us how long for the system to reach the maximum segregation. In this work, we also developed a kinetic model based on foreign atom movement in an appropriate potential, which aims at giving a consistent description of the segregation equilibria, the time and temperature dependence of surface concentration and in-depth concentration distribution. The frame work of kinetic models is referenced to the work by Hofmann and Erlewein [60]. Only some basic equations and information are described here. The model assumes negligible interface evaporation and the GB enrichment limited to the first monolayer. The potential gradient for GB segregation adopted from Hofmann and Erlewein's work is schematically shown in Figure *4*.

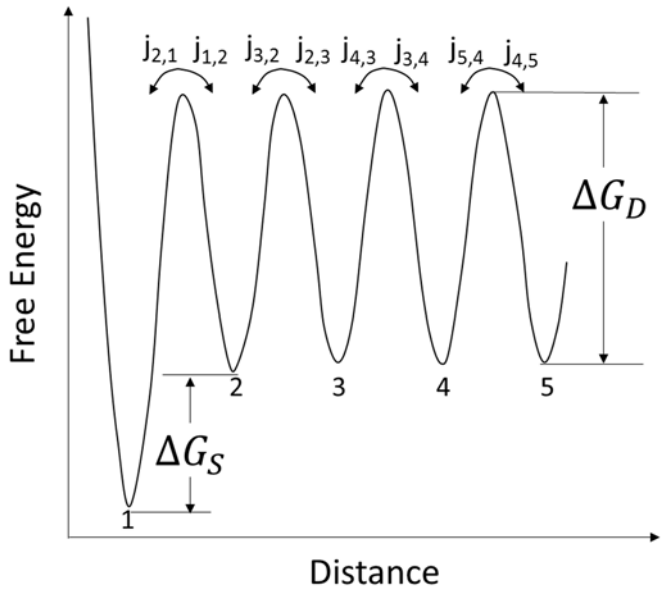

Figure 4 Assumed free energy versus depth for segregant atoms at the surface and in the bulk

Atomic fluxes based on reaction rate theory were used to describe the attainment of concentration distribution, avoiding difficulties with the solution of a diffusion equation in a potential gradient. The flux equations were described by Eq. (12a~d):

$$J_{12} = a_1^{-2} X_1 W_{12} \vartheta_1 \exp\left[-\frac{\Delta G_D - \Delta G_S}{RT}\right] \quad (12a)$$

$$J_{21} = a_1^{-2} X_2 W_{21} \vartheta_2 \exp\left[-\frac{\Delta G_D}{RT}\right] \quad (12b)$$

$$J_{23} = a_1^{-2} X_2 W_{23} \vartheta_2 \exp\left[-\frac{\Delta G_D}{RT}\right] \quad (12c)$$

…

$$J_{i,i+1} = a_i^{-2} X_i W_{i,i+1} \vartheta_i \exp\left[-\frac{\Delta G_D}{RT}\right] \quad (12d)$$

Where a_i is the atomic jump distance, X_i is the concentration of solute atoms in layer "i", ϑ_i is the solute atom oscillation frequency and $W_{i,i+1}$ is the jump probability factors of the solute atoms. In a first order approximation, all jump frequencies are assumed to be equal as well as the jump distances. The deviation for a_1 and ϑ_1 from this assumption will be accounted by segregation energy. ΔG_D is the activation energy for diffusion, and it will be derived from the experimental diffusion coefficient. ΔG_S is the segregation energy, which will be derived from either experimental data or the thermodynamic theory discussed in Section 2.1. The jump probability factor was assigned using the following relationship based on Hofmann's work:

$$w_{21} = \left(1 - \frac{X_S}{X_S^M}\right)^{X_S^M} \quad (13a)$$

$$W_{12} = 1 - X_2 \ (13b)$$

$$W_{23} = 1 - X_3 \ (13c)$$

$$W_{i,i+1} = 1 - X_{i+1} \ (13d)$$

Where X_S is surface composition and X_S^m is the maximum allowable surface coverage

Computational codes for calculating thermodynamics and kinetics of thermal segregation have been implemented using the wolfram programing language and Matlab.

4. Results and discussion

In this section, modeling results will be presented in the following sequence: 1) Thermodynamic and kinetic calculation of solute GB segregation in the Fe-P system; 2) Thermodynamic calculation of solute GB segregation in the Fe-M-P and Fe-M-C-P (M=Cr, Ni, Mn, Mo, Nb, Ti) systems. All the intrinsic segregation energies of pure elements ΔG_I^0 were taken from the *Appendix B Predicted Values of Enthalpy and Entropy of Segregation in α_Fe* in the book by Lejček [56].

4.1 Thermodynamic and kinetic calculation of thermal segregation in the Fe-P system

Based on literature review, the chemical state of segregated P is in the form of Fe_3P. Therefore, we assume that the GB structure favors that P forms covalent bonds with Fe, i.e., a two-dimensional Fe_3P structure. The energy released from such phase transformation contributes to the segregation energy. The AES measured P coverage by Erhart and Grabke [22] represents that of Fe_3P and the GB segregation energy of P in α_Fe, i.e., 34300+21.5T (J/mol) is applicable to calculate the coverage of Fe_3P. This quantity corresponds to the ΔG_I in Eq. (1), assuming negligible chemical interaction in a dilute solution. The segregation energy is independent of the bulk and surface composition. The calculated phosphorus composition at GBs (converted from the coverage of Fe_3P through Eq. (2)) is plotted as a function of alloy composition and temperature in Figure *5*(a) and (b), compared well with the experimental data from Erhart and Grabke [22]. The results calculated from thermal segregation models suggested that the segregation of P at GB increases with increasing bulk composition and decreasing temperature, which is in good agreement with experimental observation.

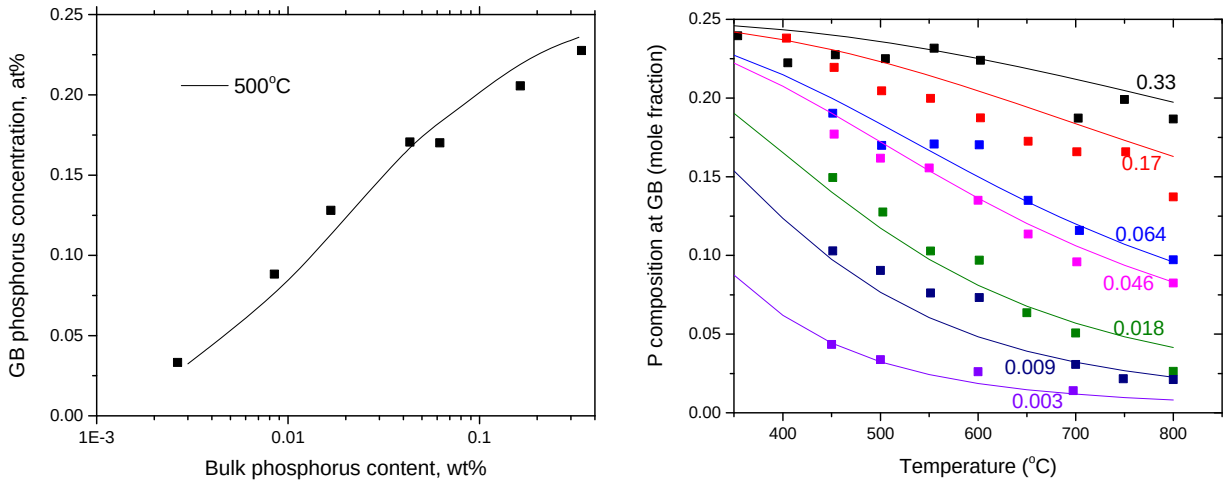

Figure 5 The equilibrium segregation of phosphorus at grain boundary (a) as a function of alloy composition (bulk phosphorus content) at 500°C, and (b) as a function of both alloy composition (wt%) and temperature, compared to the experimental data [22].

Based on the model description in Sec. 3.2, the kinetic simulation was performed for the alloys in Erhart and Grabke's work. The most important input quantities are the diffusion coefficient of P in α iron and the GB segregation energy. The same segregation energy 34300+21.5T (J/mol) was used in kinetic simulation. The phosphorus diffusion coefficient in α_Fe has been measured experimentally, i.e., $1.38*10^5$ exp(-3.4 eV/kT) cm^2/s in the temperature range (932– 1017 K) and $8*10^5$ exp(-3.2 eV/kT) cm^2/s in the temperature range (783– 923 K) [61]. The P diffusion is much larger than the self-diffusion coefficient. Indeed, at 870 K, the self-diffusion coefficient is 10^{-20} m^2/s, while the diffusion coefficient of P in ferromagnetic BCC Fe is 10^{-17} m^2/s [61]. This fact could be associated with diffusion involving interstitials rather than vacancies. Domain and Besquart did ab-initio calculation on the diffusion of P in α iron [62]. They found that the diffusion coefficient of P based on a vacancy mechanism, although less than the experimental measurement of P in α iron, had already been larger than the self-diffusion coefficient by one to three orders of magnitude. Due to the lack of quantitative description of the interstitial diffusion of P in α iron, we will use experimental diffusion coefficient data of P in α iron in this work. We then simulated the GB composition of P as a function time, temperature, and bulk composition. Critical results are now presented.

For an alloy with a high P composition of 0.33 wt% P at 723K(450°C), the calculated concentration profile of P as a function of distance from GB is plotted in Figure *6*(a). The red curve denotes the profile at 0.1h and the blue curve at 10000h. The results suggested that at the earlier stage of segregation, there is a depletion regime of P at the sub-GB region. This is because the segregation energy leads to a large flux from sub-GB region to GB plane, while at this time, the flux into the sub-GB regime was supplied by continuous diffusion from the bulk. For longer times, the GB segregation gradually reaches equilibrium, and the depleted region gradually disappears until the steady state is established.

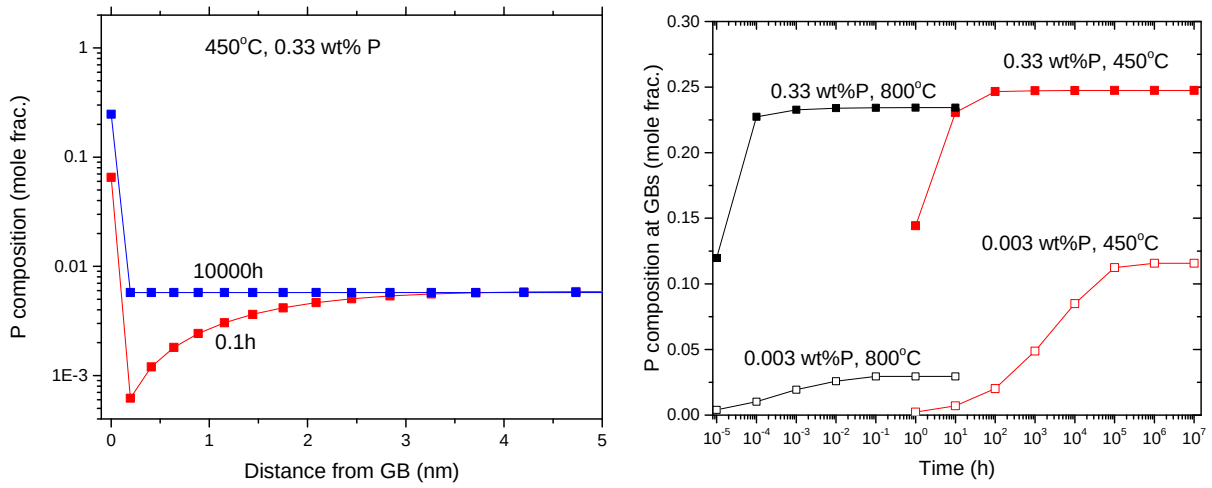

(a) (b)

Figure 6 The composition of P at GBs (a) at 450ºC for Fe-0.33wt%P as a function of distance from GB for the 0.1h and 10000h; (b) as a function of time for alloy Fe-0.33 wt%P and Fe-0.003 wt%P at 723 and 1073K (450 and 800°C), respectively.

In Figure *6*(b), the P composition at GBs as a function of time was calculated for Fe-0.33wt%P and Fe-0.003wt% P alloys at 723 and 1073K (450 and 800°C), respectively. The plateau in each curve suggests the equilibrium segregation is reached. The results show that the equilibrium segregation at 800°C is reached within 0.001~0.1h, while the time to reach equilibrium at 723K(450°C) is ~10 h for high P alloy and 10^6 h for low P alloy. The equilibrium segregation level predicted from the kinetic modeling is well consistent with the thermodynamic calculation in Figure 5 (b), indicating the kinetic modeling used a correct boundary condition for equilibrium segregation for infinitely long aging period. However, based on the kinetic simulation, it is suggested that the experimental data at low temperature 723K(450°C) for low P alloys should be used with caution to derive segregation energy as the experimental data may not reach equilibrium.

4.2 Thermodynamic of thermal segregation in the Fe-C-P system

Carbon has been found to strongly affect the P segregation, displacing P from the GBs if present with high enough activity. C is a common element in steels, therefore, it is necessary to consider P and C segregation simultaneously when dealing with real alloys.

The calculated C and P segregation as a function of C content is plotted and compared with experimental data in Figure *7*. The results show the evidence for the competition between P and C. As the C content in the bulk increases, the amount of P segregation decreases. At about 50 wt. ppm of C content, the maximum solid solubility of carbon in equilibrium with cementite is reached, and a further increase in the bulk content of C does not change the amount in α_Fe solid solution. Therefore, beyond this point, the C and P segregation are expected to be constant, and the simulation and experimental results shows a plateau is reached. The C and P concentration in most steels are within dilute limit, therefore, their segregation at GBs is mainly due to site

competition mechanism, that is, both elements compete for a limited number of sites and their segregation tendency is given by constant values of their segregation free energies. Because of the site competition mechanism, it is assumed that the calculated C segregation represents the Fe_3C coverage at GBs. In this work, the segregation energy of C in α_Fe $\Delta G_C^0 = 76000$ $(\frac{J}{Mol})$ is used. The same segregation energy of P as that in previous sections $\Delta G_P^0 = 34300 + 21.5T$ $(\frac{J}{Mol})$ is used. Although detailed kinetics analysis on segregation in Fe-C-P was not carried out, it was assumed that the experimental data can reasonably represent the equilibrium data.

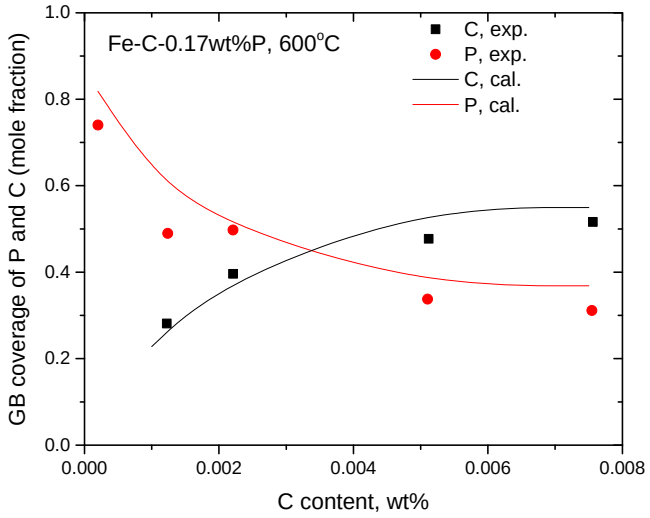

Figure 7 GB coverage of Fe_3P and Fe_3C as a function of C content in the bulk in Fe-C-P alloys

4.3 Thermodynamic calculation of solute segregation in Fe-M-P ternary and Fe-M-C-P quaternary systems (M=Cr, Mn, Ni, Mo, Nb,Ti)

To model the segregation in Fe-M-P ternary systems, we need to know how additional alloying elements influence the composition of solute in the solvent, and chemical interaction between solute and solvent. Both quantities can be calculated from thermodynamic Gibbs energy functions of phases. A thermodynamic database that includes thermodynamic Gibbs energy functions for phases in Fe-M-P and Fe-M-C-P (M=Cr, Mn, Ni, Mo, Nb, Ti) systems has been compiled and developed in this study, using the Calphad approach. It was then used to calculate thermodynamically related quantities for GB segregation of solute in the Fe-M-P and Fe-M-C-P systems. Details are given below.

4.3.1 Thermodynamic calculation on P solubility in α_Fe in Fe-M-P systems

Effect of alloying elements Cr, Ni, Mn, Mo, Nb and Ti on the solubility of P in the α_Fe solid solution have been systematically evaluated using the currently developed Fe-M-P thermodynamic database. The calculated results are plotted in Figure *8*. This plot shows the calculated solubility of P in α_Fe when the concentration of M (Cr, Ni, Mn, Mo, Nb and Ti) is 0,

0.1 and 1 wt%, respectively. For Nb and Ti, an additional level of 0.01 wt% were also calculated and plotted.

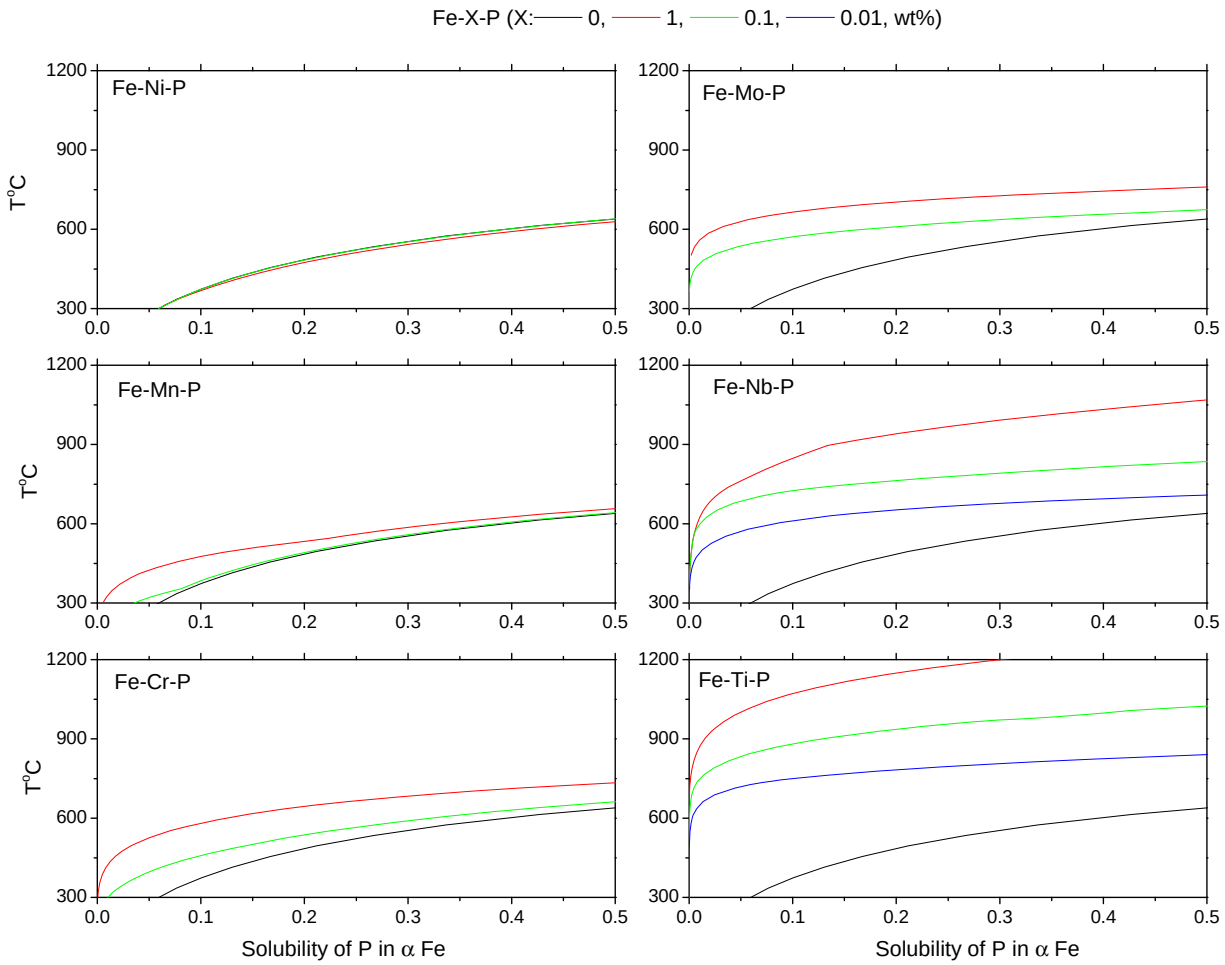

Figure 8 Effect of alloying element M (M=Cr, Mn, Ni, Mo, Nb,Ti) on solubility of P in the α_Fe solid solution

The comparison shows that Ni has negligible effect on the solubility, while Mn and Cr slightly reduce the solubility of P in α_Fe. Mo, Nb and Ti more drastically reduce the solubility of P in α_Fe than Cr, Ni and Mn. The solubility of P in α_Fe of the Fe-P binary is determined by the Gibbs free energy of α_Fe and Fe_3P. When an alloying element M is added, it can dissolve into the Fe_3P structure through the substitution with Fe, or it can form a new compound FeMP. Cr, Ni, Mn fall into the former case in which the Gibbs energy of Fe_3P becomes slightly reduced, and therefore the solubility of P in α_Fe is slightly reduced. On the other hand, Mo, Nb and Ti fall into the latter case. They form a much more stable FeMP compound than Fe_3P. This new compound is now in equilibrium with α_Fe, which greatly reduces the solubility of P in α_Fe. This is why Mo, Nb and Ti are often added as scavenging elements for P. Among them, Ti is the most efficient elements in reducing the P solubility in α_Fe. Due to the reduced concentration P in α_Fe in Mo, Nb and Ti, the anticipated P segregation at GB would also be reduced. This may explain why adding Mo, Nb and Ti can help mitigate the GB segregation of P in Fe-alloys.

4.3.2 Thermodynamic calculation on chemical interaction in α_Fe in Fe-M-P systems

The first two terms in Eqs. 8(a~b) for a dilute solution were often derived from experimental data as composition independent quantities. Therefore, the evaluation of chemical interaction is mainly to provide knowledge on the third term which is in the form of $(L_{FeP} + L_{FeM} - L_{MP})$. Therefore, we need to know the chemical interaction of Fe-P, Fe-M and M-P. The chemical interaction between elements will be demonstrated through the activity vs composition plot. The activity of M in α_Fe at 800°C is plotted in Figure *9*(a). The straight diagonal line represents an ideal solid solution in which there no chemical interaction between Fe and M. The McLean equation can be perfectly applied to this case. The calculated results show that the elements can be divided into three groups. This first group includes Mn, Ni, Nb. Their activity curves are close to the straight diagonal line, suggesting that these systems display an approximately ideal behavior. Therefore, the chemical interaction between M (M=Mn, Ni, Nb) and Fe can be neglected. The second group includes Cr and Mo that display a positive deviation from the ideal behavior. The positive interaction means that different elements do not want to mix with each other. They tend to form phase separation. This is why we see phase separation in the Fe-Cr system. The positive interaction promotes the GB segregation of solute atoms. The third group consists of Ti, displaying a negative deviation from ideal behavior, suggesting a strong tendency for mixing between Fe and Ti. The chemical interaction between M-P is demonstrated by the activity of P in α_Fe versus P composition in the bulk in Figure *9*(b). All M-P systems display negative deviation from ideal behavior, suggesting negative interaction or strong mixing between metal elements and P. The Fe-P is highlighted in bold line in Figure *9*(b). Although all individual M-P systems show large negative interaction, their contribution to the segregation energy is not so great, because based on the formula of $(L_{FeP} + L_{FeM} - L_{MP})$, the difference between L_{FeP} and L_{MP} is more relevant. In addition, thermodynamic modeling of the M-P systems is considered less reliable than that of the Fe-M system. In this work, we assume that the M-P interaction is largely canceled by the Fe-P interaction. Therefore, the third term is mainly determined by the Fe-M interaction. Based on thermodynamic analysis here, the chemical interaction in the Fe-Ni, Fe-Mn, and Fe-Nb systems can be ignored. There is positive contribution to the interaction energy in the Fe-Cr and Fe-Mo cases. For the P segregation energy in the Ti case, $(L_{FeP} + L_{FeM} - L_{MP})(x_M^{\varphi} - x_M^{B})$, although there is large negative interaction, this term can be ignored. Because Ti forms a very stable FeMP compound, which efficiently reduced the concentration of Ti in α_fe to a negligible level. Because the nature of negative interaction, the concentration of Ti at GBs is also negligible. Therefore, the third term in Eqs. 8(a~b) can be ignored. For the same reason, the Ti segregation is neglected in the Fe-Ti-P alloys. Since only the knowledge on the chemical interaction in the α_Fe solid solution is needed, all other phases were suspended in the calculation.

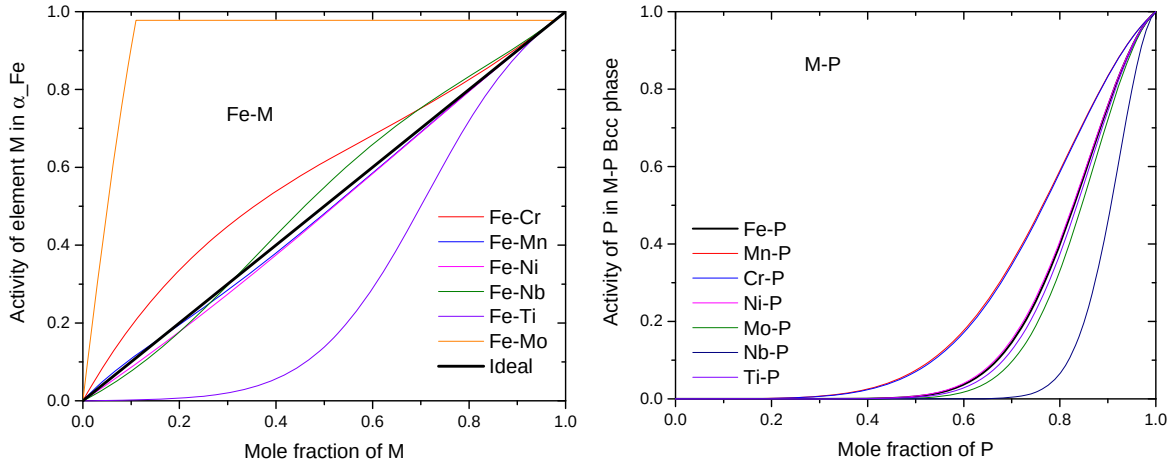

Figure 9 (a) Activity of M (M=Cr, Mn, Ni, Mo, Nb,Ti) in the α_Fe solid solution in the Fe-M systems as a function of M content in the bulk, (b) activity of P in the α_Fe solid solution in the M-P systems as a function of P content in the bulk

4.3.3 Thermodynamic calculation of solute GB segregation in the Fe-C-P, Fe-M-P and Fe-M-C-P systems (M=Cr, Mn, Ni, Mo, Nb, Ti)

Next, we will consider metal alloying elements Cr, Mn, Ni, Mo, Nb, Ti on the P segregation at GBs of α_Fe in Fe-M-P and Fe-M-C-P systems. All these elements except Ni tend to reduce the solubility of C in the solid solution by forming metal carbides such as $Cr_{23}C_6$, $Mn_{23}C_6$, MoC, NbC and TiC. Ni can stabilize Fe_3C by dissolving into this structure, which also helps to reduce the C solubility in α_Fe. Based on the stability of the carbides, the potency in C solubility reduction is in the order of Ni<Mn<Cr<Mo<Nb<Ti. The more potent the element, the less amount is needed to bind the C atoms. The direct consequence of the C reduction is to promote the P segregation due to less C atoms competing for the GB sites with P. However, these alloying elements also interact with P atoms, in both situations with or without C present. Based on the effects of reducing the P solubility and forming chemical interactions with P, the alloying elements were divided into three categories and treated with different approaches. The first category Mn and Ni was treated by simple McLean equations, assuming negligible solubility reduction and chemical interaction; the second category Cr and Mo were treated with the Guttmann equation by including a positive interaction term after the solubility reduction effect; the third category Nb and Ti were mainly used for scavenging effect, i.e., to reduce the solubility of P in α_Fe. The remaining content of Nb or Ti in α_Fe is so small that it was not included in subsequent segregation calculation.

Fe-Cr-P, Fe-Mo-P and Fe-Cr-C-P

Based on the segregation energy of Cr in Fe-Cr dilute solution $\Delta G^0_{Cr} = 13000 - 9T\ (\frac{J}{Mol})$ and the interaction parameter between Fe and Cr $L_{FeCr} = 20500 - 9.68 * T\ (\frac{J}{mol})$, the GB

segregation of P and Cr was calculated for an Fe-Cr-P alloy containing 2.2 wt% Cr and 0.048 wt% P, and compared with experimental results [22] in Figure *10*(a). Both P and Cr were found to be enriched in the GBs of this alloy. Thermodynamic calculation shows that the Fe-0.048 wt% P alloy with a 2.2 wt% addition of Cr is in the α_Fe single phase region. It does not reduce the solubility of P in α_Iron. It is also found that the P segregation in the Fe-Cr-P alloy is almost the same as that in an equivalent Fe-0.043 wt% P binary alloy, suggesting the Cr addition does not enhance the segregation of P. On the other hand, the P segregation does enhance the Cr segregation at GBs due to the positive interaction between Fe and Cr as well as the large composition difference of P at GBs and in the bulk. It is also found that the Cr enrichment at GB only slightly increases with decreasing temperatures.

For the Fe-Mo-P system, the segregation energy of Mo in Fe-Mo dilute solution $\Delta G^0_{Mo} = 28000 - 23T\ (\frac{J}{Mol})$ and the interaction parameter between Fe and Mo $L_{FeMo} = 36818 - 9.14T\ (\frac{J}{mol})$ were used for calculation. The calculated results in Figure *10*(b) shows that Mo is enriched at GB sites similar to the enrichment of Cr. The larger the P segregation, the higher enrichment ratio versus the Mo content. On the other hand, the experimental data [46] suggested that Mo has negligible effect on P segregation. One reason that can explain the difference is that the Mo reacts with other impurity atoms such as C in the real alloys. Therefore, they were not able to efficiently reduce the P content in α_Fe. No impurity elements were considered in the calculation.

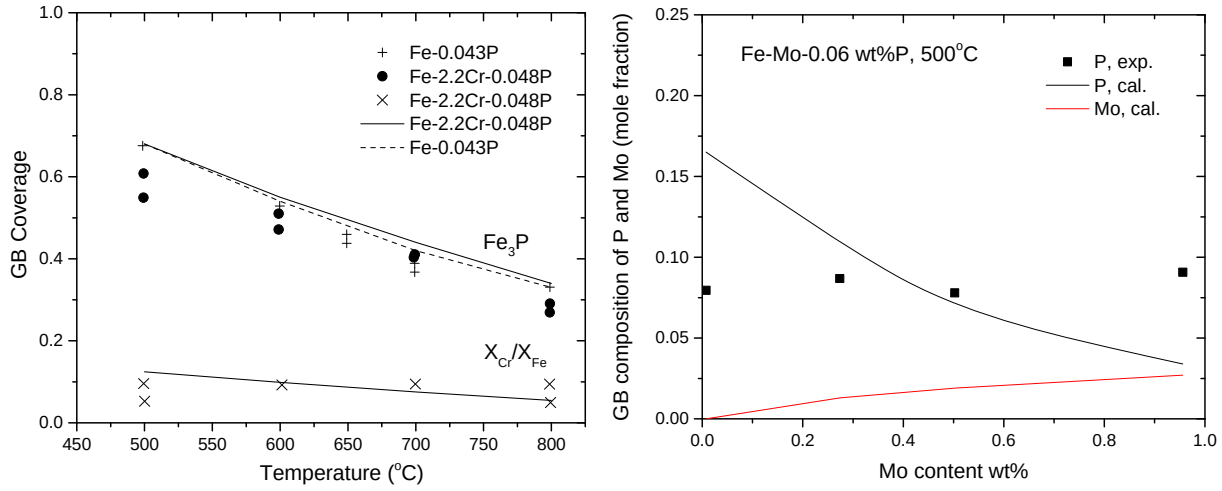

(a) (b)

Figure 10(a) GB coverage of Fe_3P and GB composition of Cr as a function of temperature in a Fe-Cr-P alloy, (b) GB composition of Mo and P as function of Mo content in the bulk in Fe-Mo-P alloys

Modeling results on segregation of C and P in Fe-0.1 wt% C-0.045 wt% P and Fe-2.2 wt% Cr-0.1 wt% C-0.047 wt% P at different temperatures are plotted in Figure *11* and compared with experimental data [22]. It is found that Cr addition has dramatic influence on the C and P segregation. First, Cr is a carbide former, which reduces the C content in solid solution, and subsequently the available C for GB segregation. Therefore, the P segregation is enhanced due to less C to compete for the GB sites. The experimental and modeling data in Figure *11* in general

demonstrate such a trend, i.e., the P segregation is greater in alloys with Cr addition, while that of C is lower in alloys with Cr addition. The simulation also shows that P segregation in the Fe-Cr-C-P alloy doesn't monotonically decrease with temperature. This is because that Cr at low temperature forms a more stable compound $(Fe,Cr)_2P$ than carbide. The formation of $(Fe,Cr)_2P$ reduces the content of P in α_Fe solid solution. Therefore, less P is available for GB segregation. Although the reduction in experimental P segregation data is not as great at that observed from modeling, the trend is consistent.

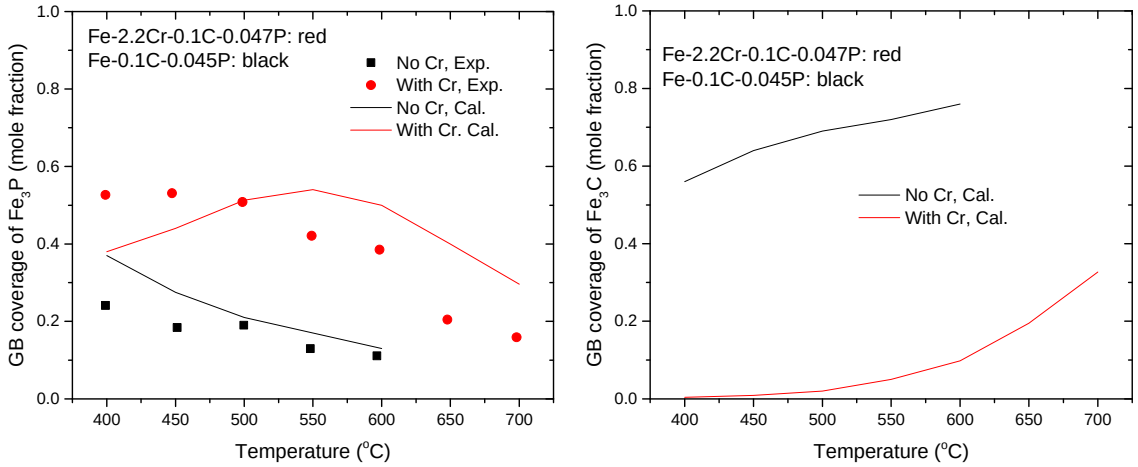

Figure 11 GB coverage of (a) Fe_3P and (b) Fe_3C as a function of temperature in a Fe-Cr-C-P alloy

Fe-Mn-P, Fe-Ni-P and Fe-Mn-C-P

To model the segregation in Fe-Mn-P and Fe-Ni-P systems, segregation energies of $\Delta G^0_{Mn} = 26000 - 23T$ $(\frac{J}{Mol})$ and $\Delta G^0_{Ni} = 20000 - 16T$ $(\frac{J}{Mol})$ were used in the calculation. Assuming the interaction of L_{FeP} and L_{MnP} can be canceled with each other, and L_{FeMn} is zero, i.e., ideal behavior, the contribution to segregation energy from chemical interaction between elements can be ignored. The calculated P segregation for Fe-(0.5~9.39) Mn-0.05P (wt%) at 500°C is shown and compared with experimental data in Figure *12*(a). The results suggest that the Mn content in the bulk has little effect on the P segregation, which is in good agreement with experimental observation. The difference in segregation magnitude between calculation and modeling may be due to the conversion method from AES signal to composition, or the presence of impurity elements such as C or S. The results also suggest that the Mn itself does not segregate at GBs. However, in literature, Mn has been frequently observed to be enriched at GB. The discordance between the experiments and simulation may be resulted from the smaller intrinsic segregation of Mn used in the calculation. Since accurate segregation data of Mn is not available from experiments due to the Mn peak overlapping with Fe in AES analysis, no attempt was made to optimize the segregation energy. There is no systematic experimental work on the segregation in Fe-Ni-P system. Doig and Flewitt provided one data point for P segregation in the Fe-3wt%Ni-0.06wt%P annealed at 550°C. They mentioned that no obvious composition change for Ni across

GBs, suggesting no co segregation between Ni and P. Following the same method as Fe-Mn-P, the calculate P and Ni segregation is shown in Figure *12*(b), in which P segregation is independent of the Ni content in alloys. Weng and McMahon [63] studied P segregation in Fe-Ni-P, Fe-Mn-P and Fe-Cr-P, for a fixed Ni, Mn and Cr content and two levels of P content. They found that P segregation mainly depended on the P content in the bulk. The Cr, Mn and Ni do not influence the segregation significantly. The comparison between calculated and experimental results is shown in Figure *13*, in which the main feature of P segregation was reflected.

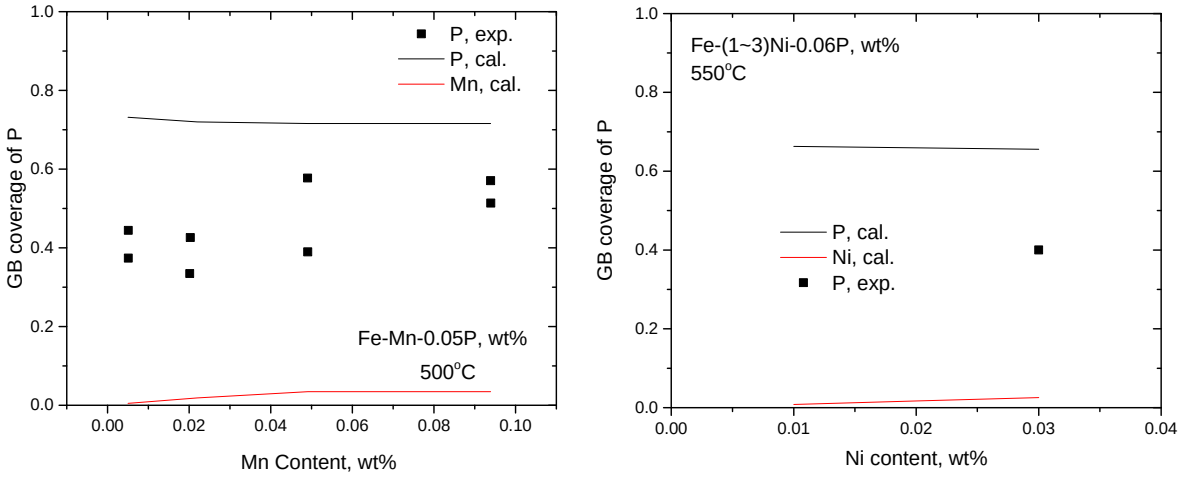

Figure 12(a) GB coverage of Fe_3P and Mn as a function of Mn content in Fe-Mn-P alloys (b) GB coverage of Fe_3P and Ni as a function of Ni content in Fe-Ni-P alloys

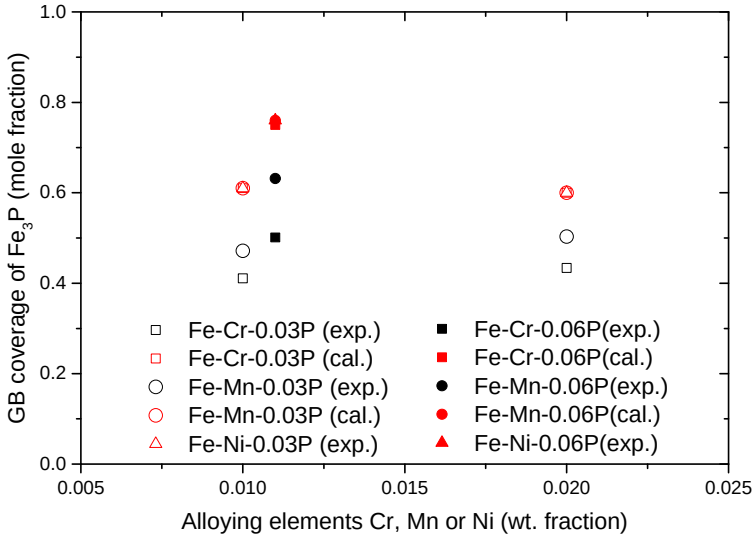

Figure 13 GB coverage of Fe_3P as a function of Mn, Cr or Ni content in the bulk for Fe-Cr-P, Fe-Mo-P and Fe-Ni-P alloys.

Experimental results were also available for the Fe-Mn-C-P system. Therefore, modeling on P and C segregation in a series of Fe-(0.5~9.39) wt% Mn-0.05 wt% P-0.15 wt% C alloys were simulated and compared with experimental data [50] in Figure *14*. Mn addition will scavenge C atoms in α_Fe solid solution by forming $Mn_{23}C_6$, leaving less C to compete with P for GB sites. Therefore, increasing Mn content leads to higher P segregation at GBs, as shown in Figure *14*. The C segregation decreases simultaneously with Mn, until the solubility of C in α_Fe is reached. At this point, further addition won't be able to reduce the C solubility, therefore, the segregation of both C and P reaches plateau.

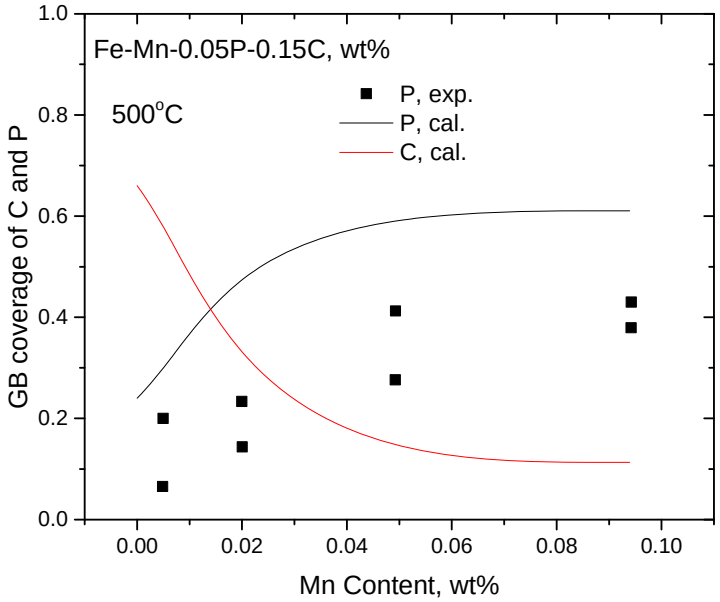

Figure 14 GB coverage of Fe_3C and Fe_3P as a function of Mn content in the bulk for Fe-Mn-C-P alloys.

Fe-Nb-P, Fe-Ti-P, Fe-Nb-C-P and Fe-Ti-C-P

Nb forms a stable intermetallic compound FeNbP in the Fe-Nb-P alloys. The formation of such a compound depletes the solute P and Nb in α_Fe, thereby, reduces the segregation of P at GB. The P segregation in Fe-Nb-P alloys was calculated in Figure *15*(a) and compared with experimental data. The remaining Nb in α_Fe is so small that it was not included in subsequent segregation calculation. While the calculated values are larger than the experimental data, both sets of data show the same trend, i.e., the P segregation was found to decrease with increasing Nb. The difference between experimental and calculated data might be also due to impurity presented in real alloys but not in calculation conditions. Ti has the similar but even stronger scavenger effect as Nb. For example, at 550°C, 0.1 wt% Ti can almost completely suppress the P segregation at GBs, as shown in Figure *15*(b).

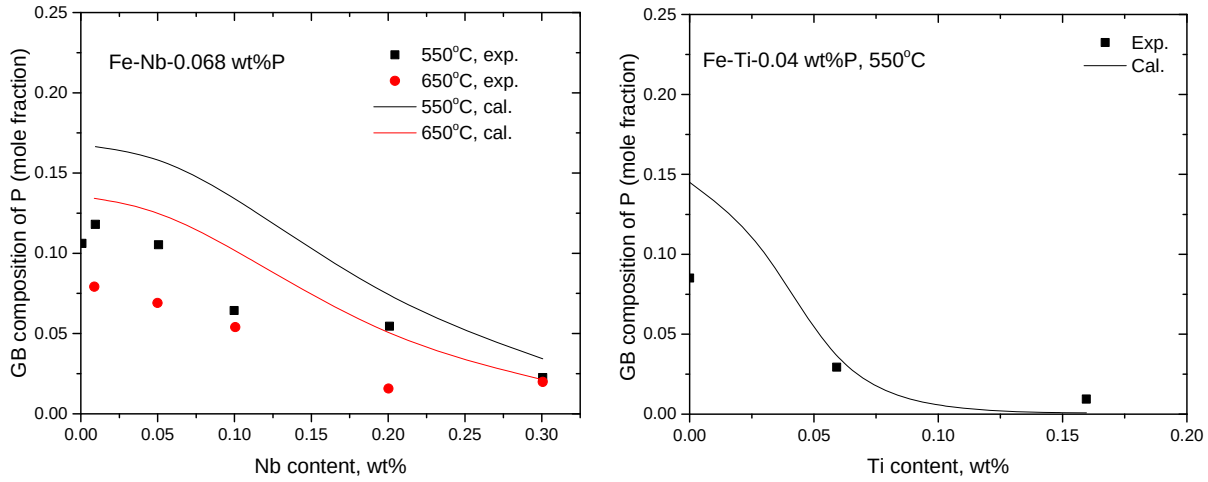

(a) (b)

Figure 15 GB composition of P in(a) Fe-Nb-P and (b) Fe-Ti-P alloys as a function of Nb or Ti content in the bulk.

Modeling results on P and C segregation in the Fe-0.3 wt%Nb-0.062 wt%P-(0.0027~0.076) wt%C alloys were presented and compared with experimental data in Figure *16*(a). Both sets of results show that a maximum of P segregation occurs at the C content of ~0.03 wt%. For the C content below this value, the P segregation dramatically decreases with decreasing C. This is due to two factors. On one hand, when C is low, almost all C is used to form NbC. Therefore, no C competes with P for GB sites, leading to maximum amount of P segregation. On the other hand, when C is very low, it is not enough to bind all Nb. The Nb atoms will form the FeNbP compound or clusters, leading to reduced segregation of P at GBs. When the C higher than 0.03 wt%, all Nb has been consumed. Upon further addition of C, the displacing effect of C becomes effective, leading to decreasing P segregation at GBs. This can be clearly demonstrated in the C segregation plot in Figure *16*(b). Despite of quantitative difference between calculated and experimental data, the modeling accurately captured the trend of segregation in the Fe-Nb-C-P alloys.

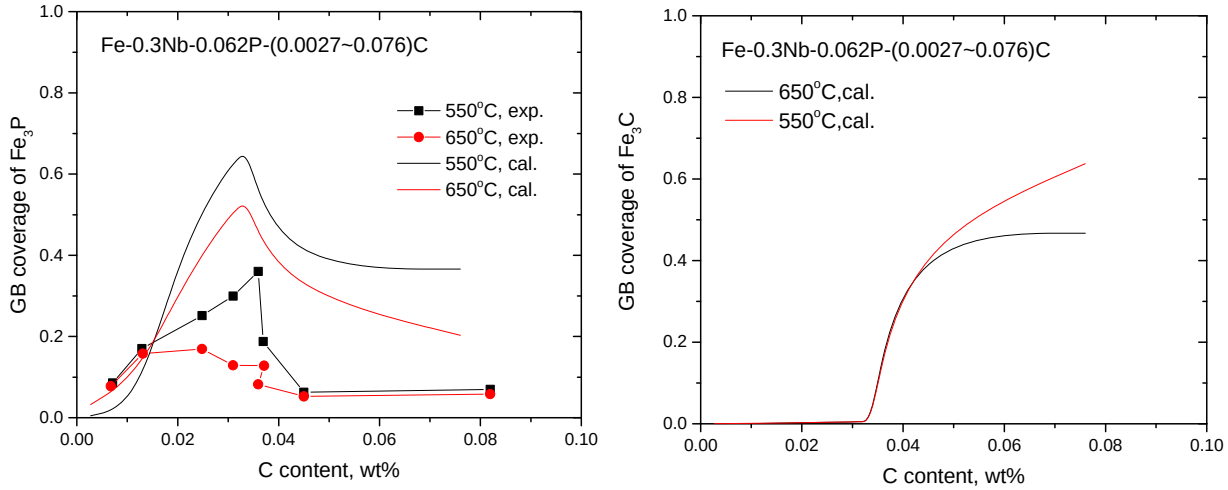

(a) (b)

Figure 16 GB coverage of (a) Fe_3P and (b) Fe_3C as a function of the C content in Fe-Nb-C-P alloys

Modeling results on Fe-0.2 wt%Ti-0.05 wt%P-(0~0.1) wt% C alloys are plotted and compared with experimental data in Figure *17*. The P segregation progressively decreases with increasing C content. The hump presented in the Fe-Nb-C-P alloys is missing in the modeling results of Fe-Ti-C-P alloys. The segregation at low content is similar to that of Fe-Nb-C-P, i.e., two factors affecting the P segregation. First, the C in the solid solution has been depleted by the formation of TiC. Less C leads to increased P segregation. But at very low C content, the amount of C is not enough to bind all Ti atoms. Therefore, Ti will form FeTiP and thereby reduce the segregation of P. However, at higher C content, there is no decreasing stage before the segregation reaches a plateau. This is because the addition of Ti leads to much smaller solubility of C and P in α_Fe solid solution. The C content at the hump point is coincident with that solubility of C, therefore, the segregation after hump point directly goes into the equilibrium stage.

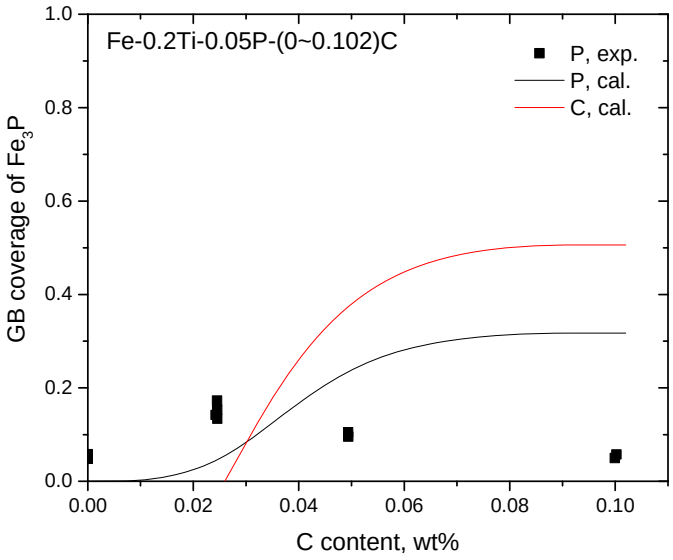

Figure 17 GB coverage of (a) Fe_3P and (b) Fe_3C as a function of the C content in Fe-Ti-C-P alloys

In summary, in the Fe-M-P ternary and Fe-M-C-P quaternary alloys many elemental interactions are possible. However, these can be understood and predicted based on our knowledge of binary and ternary systems. In multicomponent steels, the P and C segregation in steels can be understood through the site competition mechanism. Nevertheless, additional alloying elements have a profound effect on the composition of C and P in α_Fe solid solution, which in combination with the chemical interaction between alloying and matrix elements greatly affects the segregation of elements in steels.

5. Discussion on the approaches

The current approach integrated computational thermodynamics with GB segregation, in which uncertainties could come from several sources. First of all, the thermodynamic database

for the Fe-M-C-P (M= Cr, Mn, Ni, Mo, Nb, Ti) systems were developed from and validated by available experimental data based on the CALPHAD approach. Most experimental data were from high temperature thermal treatment to ensure the attainment of the equilibrium state. The low temperature phase equilibrium was calculated from the Gibbs energy functions that were extrapolated from high temperature regime. In addition, for systems with very limited solubility of P in the α_Fe solid solution such as Ti-P and Nb-P, the interaction action energy cannot be reliably modeled due to the lack of accurate solubility data. Therefore, these factors can introduce uncertainties on the solubility of solute atoms in the α_Fe solid solution at low temperature. Second, when solute atoms form a dilute non-regular solid solution with Fe, the segregation energy of pure element $\Delta G_I^0 + \Delta G^E$ should be a composition dependent quantity, i.e., a function of GB composition of solute elements. In this work, a constant segregation energy that averages the segregation over the compositions was used to reflect the experimental observation. Thirdly, for the systems with non-negligible chemical interaction, regular solution behavior is assumed, which is not necessary the case in the really alloys. For the Fe-C-P, Fe-M-P and Fe-M-C-P system, only equilibrium segregation was calculated and compared with experimental data, which is based on the assumption that kinetics is fast enough to reach equilibrium segregation in experimental alloys. While this is generally a valid assumption for most experimental conditions, it should be excised with caution on very low P containing alloys at very low temperature. Detailed kinetic analysis and modeling is certainly desired for ternary and quaternary alloys, which is currently ongoing.

6. Summary of conclusions

The major outcomes from this work are listed in the following:

1) Multicomponent thermodynamic database of Fe-M-C-P (M=Cr, Mn, Ni, Mo, Nb, Ti) has been compiled and developed based on critically assessed literature data. This database provided major thermodynamic inputs for thermal GB segregation model.
2) The McLean equation was used to describe the GB segregation of an ideal solid solution, and the Guttmann's equation was used to describe the GB segregation of non-ideal solid solution of multicomponent alloys.
3) For different alloying additions (M=Cr, Mn, Ni, Mo, Nb, Ti), the solubility of P in α_Fe was systematically evaluated, and the solid solution behavior of Fe-M and M-P was also assessed to provide guidance on the selection of GB segregation model.
4) Among the six alloying elements (M=Cr, Mn, Ni, Mo, Nb, Ti), Mn and Ni do not affect the P segregation. The currently used intrinsic segregation energy of Mn and Ni suggests that they do not segregate at GBs. Cr and Mo do not affect the segregation of P either, however, unlike Mn and Ni, they will enrich at GBs due to positive or repulsive interaction with the matrix Fe atoms. Nb and Ti greatly reduces the P segregation due to the very strong scavenging effect. The remaining Nb and Ti in α_Fe are so small that they were not included in GB segregation modeling.
5) C strongly affects the P segregation, by competing with P for GB sites. Additions of alloying elements such Cr, Ni, Mn, Mo, Nb and Ti, on one hand, can scavenge the C atoms in solid solution by forming M carbides. Less C in solid solution leads to weaker competition of C for GB sites, thereby promoting the segregation of P. On the other hand,

these metal additions may simultaneously reduce the P solubility by forming metal phosphides, which helps to suppress the P segregation. Therefore, P segregation displays a more complex behavior in the Fe-M-C-P systems.

7. Future work

The following work is planned in the next step:

1) Additional sensitivity test on the parameters used in this modeling will be performed.
2) Kinetic analysis and modeling for ternary Fe-M-P and quaternary Fe-M-C-P alloys (M=Cr, Mn, Ni, Mo, Nb and Ti) is desired.
3) Integrate the thermal segregation code with irradiation-induced segregation code to simulation segregation of steels used in nuclear reactors.

8. References

1. Allen, T. and J. Busby, *Radiation damage concerns for extended light water reactor service.* JOM, 2009. **61**(7): p. 29-34.
2. Fukuya, K., *Current understanding of radiation-induced degradation in light water reactor structural materials.* Journal of Nuclear Science and Technology, 2013. **50**(3): p. 213-254.
3. Garner, F., *4.02-Radiation Damage in Austenitic Steels,"*. 2012, Oxford: Elsevier. p. 33-95.
4. Kenik, E.A. and J.T. Busby, *Radiation-induced degradation of stainless steel light water reactor internals.* Materials Science and Engineering: R: Reports, 2012. **73**(7): p. 67-83.
5. Zinkle, S.J. and G. Was, *Materials challenges in nuclear energy.* Acta Materialia, 2013. **61**(3): p. 735-758.
6. Allen, T.R. and G. Was, *Modeling radiation-induced segregation in austenitic Fe–Cr–Ni alloys.* Acta materialia, 1998. **46**(10): p. 3679-3691.
7. Field, K.G., et al., *Defect sink characteristics of specific grain boundary types in 304 stainless steels under high dose neutron environments.* Acta Materialia, 2015. **89**: p. 438-449.
8. Hashimoto, T., Y. Isobe, and N. Shigenaka, *A model for radiation-induced segregation in fcc binary alloys.* Journal of nuclear materials, 1995. **225**: p. 108-116.
9. Lam, N., *Compositional changes in Fe-Cr-Ni alloys under proton bombardment at elevated temperatures.* Journal of Nuclear Materials, 1983. **117**: p. 106-112.
10. Marwick, A., *Segregation in irradiated alloys: the inverse Kirkendall effect and the effect of constitution on void swelling.* Journal of Physics F: Metal Physics, 1978. **8**(9): p. 1849.
11. Takahashi, H. and N. Hashimoto, *Radiation-induced segregation and grain boundary migration in Fe–Cr–Ni model alloy under irradiation.* Materials Transactions, JIM, 1993. **34**(11): p. 1027-1030.
12. Watanabe, S., et al., *Quantitative studies of irradiation-induced segregation and grain boundary migration in Fe Cr Ni alloy.* Journal of nuclear materials, 1995. **224**(2): p. 158-168.
13. Wiedersich, H., P. Okamoto, and N.Q. Lam, *A theory of radiation-induced segregation in concentrated alloys.* Journal of Nuclear Materials, 1979. **83**(1): p. 98-108.
14. Yang, Y.F., Kevin; Allen, Todd; and Busby, Jeremy, *Roles of Vacancy/Interstitial Diffusion and Segregation in the Microchemistry*

at Grain Boundaries of Irradiated Fe-Cr-Ni alloys Journal of Nuclear materials, 2016. **Submitted**.
15. Perks, J., A. Marwick, and C. English, *A computer code to calculate radiation-induced segregation in concentrated ternary alloys.* 1986.
16. Lukas, H.L., S.G. Fries, and B. Sundman, *Computational thermodynamics: the Calphad method*. Vol. 131. 2007: Cambridge university press Cambridge.
17. Busby, J., et al. *Influence of initial grain boundary composition on the evolution of radiation-induced segregation profiles*. in *MRS Proceedings*. 1998. Cambridge Univ Press.
18. Cole, J.I., et al. *The Influence of Pre-Irradiation Heat Treatments on Thermal Non-Equilibrium and Radiation-Induced Segregation Behavior in Model Austenitic Stainless Steel Alloys*. in *Effects of Radiation on Materials: 21st International Symposium*. 2004. ASTM International.
19. Nastar, M. and F. Soisson. *Radiation-induced segregation*. 2012. Elsevier B.V.
20. McMahon Jr, C. and L. Marchut, *Solute segregation in iron-based alloys.* Journal of Vacuum Science & Technology, 1978. **15**(2): p. 450-466.
21. Briant, C. and R. Mulford, *Surface segregation in austenitic stainless steel.* Metallurgical Transactions A, 1982. **13**(5): p. 745-752.
22. Erhart, H. and H. Grabke, *Equilibrium segregation of phosphorus at grain boundaries of Fe–P, Fe–C–P, Fe–Cr–P, and Fe–Cr–C–P Alloys.* Metal Science, 1981. **15**(9): p. 401-408.
23. Guttmann, M., P. Dumoulin, and M. Wayman, *The thermodynamics of interactive co-segregation of phosphorus and alloying elements in iron and temper-brittle steels.* Metallurgical Transactions A, 1982. **13**(10): p. 1693-1711.

24. Hänsel, H. and H.J. Grabke, *Grain boundary segregation of phosphorus and carbon in ferritic iron.* Scripta metallurgica, 1986. **20**(11): p. 1641-1644.
25. Hondros, E. *The influence of phosphorus in dilute solid solution on the absolute surface and grain boundary energies of iron*. in *Proceedings of the Royal Society of London A: Mathematical, Physical and Engineering Sciences*. 1965. The Royal Society.
26. Suzuki, S., K. Abiko, and H. Kimura, *Phosphorus segregation related to the grain boundary structure in an Fe□ P alloy.* Scripta Metallurgica, 1981. **15**(10): p. 1139-1143.
27. Suzuki, S., et al., *Effect of carbon on the grain boundary segregation of phosphorus in α-iron.* Scripta metallurgica, 1983. **17**(11): p. 1325-1328.
28. Viswanathan, R., *Temper embrittlement in a Ni-Cr steel containing phosphorus as impurity.* Metallurgical Transactions, 1971. **2**(3): p. 809-815.
29. Brimhall, J., D. Baer, and R. Jones, *Effect of irradiation on phosphorus segregation.* Journal of Nuclear Materials, 1983. **117**: p. 218-223.
30. Druce, S.G., et al. *The modelling of irradiation-enhanced phosphorus segregation in neutron irradiated reactor pressure vessel submerged-arc welds*. in *Effects of Radiation on Materials: 17th International Symposium*. 1996. ASTM International.
31. Faulkner, R., et al., *Grain boundary segregation under neutron irradiation in dilute alloys.* Journal of nuclear materials, 1998. **255**(2): p. 189-209.
32. Gurovich, B., et al., *Intergranular and intragranular phosphorus segregation in Russian pressure vessel steels due to neutron irradiation.* Journal of nuclear materials, 2000. **279**(2): p. 259-272.
33. Nishiyama, Y., et al., *Effects of neutron-irradiation-induced intergranular phosphorus segregation and hardening on embrittlement in reactor pressure vessel steels.* Acta Materialia, 2008. **56**(16): p. 4510-4521.
34. Song, S.-H., et al., *Grain boundary phosphorus and molybdenum segregation under irradiation and thermal conditions in a 2.25 Cr1Mo steel.* Materials Science and Engineering: A, 2000. **286**(2): p. 230-235.
35. Watanabe, H., et al., *Effects of phosphorus on defect behavior, solute segregation and void swelling in electron irradiated Fe□ Cr□ Ni alloys.* Journal of Nuclear Materials, 1988. **155**: p. 815-822.
36. Ramasubramanian, P. and D. Stein, *An investigation of grain-boundary embrittlement in Fe− P, Fe− P− S, and Fe− Sb− S alloys.* Metallurgical Transactions, 1973. **4**(7): p. 1735-1742.
37. Matsuyama, T. and H. Suto, *Equilibrium Grain Boundary Segregation of P in Fe–P Binary Alloys.* Transactions of the Japan Institute of Metals, 1979. **20**(2): p. 44-50.
38. Oku, M., et al., *Study of chemical states at intergranular fracture planes of iron-phosphorus alloys by auger and electron energy-loss spectroscopies.* Journal of electron spectroscopy and related phenomena, 1984. **34**(1): p. 55-65.
39. Abiko, K., S. Suzuki, and H. Kimura, *Chemical state of phosphorus segregated at grain boundaries of iron.* Tetsu-to-Hagane(J. Iron Steel Inst. Jpn.), 1983. **69**(6): p. 625-630.
40. Egert, B. and G. Panzner, *Electron spectroscopic study of phosphorus segregated to α-iron surfaces.* Surface Science, 1982. **118**(1-2): p. 345-368.
41. Hashimoto, M., et al., *Atomistic studies of grain boundary segregation in Fe-P and Fe-B alloys—I. Atomic structure and stress distribution.* Acta Metallurgica, 1984. **32**(1): p. 1-11.
42. Hashimoto, M., et al., *Transformation of the grain boundary structure in iron by phosphorus segregation.* Scripta Metallurgica, 1982. **16**(3): p. 267-270.
43. Ishida, Y. and M. Mori, *Theoretical studies of segregated internal interfaces.* Le Journal de Physique Colloques, 1985. **46**(C4): p. C4-465-C4-474.
44. Davis, L.E., et al., *Handbook of Auger electron spectroscopy.* Physical Electronics Industries, Eden Prairie, MN, 1976. **27**: p. 61-93.
45. Briant, C. and H.J. Grabke. *Grain Boundary Segregation in Iron and Its Alloys and Its Effect on Intergranular Fracture*. in *Materials Science Forum*. 1989. Trans Tech Publ.

46. Grabke, H., et al., *Effects of the alloying elements Ti, Nb, Mo and V on the grain boundary segregation of P in iron and steels.* Surface and interface analysis, 1987. **10**(4): p. 202-209.
47. Doig, P. and P. Flewitt, *Microanalysis of Grain Boundary Segregation in Embrittled Iron-3wt% Nickel Alloys Using STEM.* Journal of Microscopy, 1978. **112**(3): p. 257-267.
48. Grabke, H. and C. Briant, *Comments on "About the existence of grain boundary cosegregation in pure FeMI solid solutions".* Scripta metallurgica, 1988. **22**(7): p. 1169-1172.
49. Briant, C., *The effect of nickel, chromium, and manganese on phosphorus segregation in low alloy steels.* Scripta Metallurgica, 1981. **15**(9): p. 1013-1018.
50. Grabke, H., et al., *Effects of manganese on the grain boundary segregation, bulk and grain boundary diffusivity of P in ferrite.* Scripta metallurgica, 1987. **21**(10): p. 1329-1334.
51. Tatsumi, K., N. Okumura, and M. Yamamoto, *The effect of manganese on intergranular fracture in low alloy steels.* Le Journal de Physique Colloques, 1988. **49**(C5): p. C5-699-C5-704.
52. Möller, R. and H. Grabke, *Grain boundary segragation of phosphorus in Fe□ Nb□ P and Fe□ Nb□ C□ P alloys.* Scripta metallurgica, 1984. **18**(5): p. 527-530.
53. Guttmann, M., et al., *Interfacial segregation.* ASM, Metals Park, OH, 1979: p. 261.
54. Fowler, R.H. and E.A. Guggenheim, *Statistical thermodynamics.* 1941.
55. Guttmann, M., *Equilibrium segregation in a ternary solution: A model for temper embrittlement.* Surface Science, 1975. **53**(1): p. 213-227.
56. Lejcek, P., *Grain boundary segregation in metals*. Vol. 136. 2010: Springer Science & Business Media.
57. Kaptay, G., *Modelling equilibrium grain boundary segregation, grain boundary energy and grain boundary segregation transition by the extended Butler equation.* Journal of Materials Science, 2016. **51**(4): p. 1738-1755.
58. Butler, J., *The thermodynamics of the surfaces of solutions.* Proceedings of the Royal Society of London. Series A, Containing Papers of a Mathematical and Physical Character, 1932. **135**(827): p. 348-375.
59. Yang, Y., *Thermodynamic and Kinetic Modeling on Thermal Segregation of Phosphorus in Iron*. 2016, Oak Ridge National Laboratory (ORNL), Oak Ridge, TN (United States).
60. Hofmann, S. and J. Erlewein, *A model of the kinetics and equilibria of surface segregation in the monolayer regime.* Surface Science, 1978. **77**(3): p. 591-602.
61. Le Claire, A. and G. Neumann, *Diffusion of Impurities in Solid Metallic Elements, Chap. 3 in: Diffusion in Solid Metals and Alloys, H. Mehrer (Vol. Ed.), Landolt-Börnstein, Numerical Data and Functional Relationships in Science and Technology, New Series Vol. III/26*. 1990, Springer-Verlag.
62. Domain, C. and C. Becquart, *Diffusion of phosphorus in α− Fe: An ab initio study.* Physical Review B, 2005. **71**(21): p. 214109.
63. Yu-Qing, W. and C. McMahon, *Interaction of phosphorus, carbon, manganese, and chromium in intergranular embrittlement of iron.* Materials science and technology, 1987. **3**(3): p. 207-216.